Journal of Applied Physics

Effect of varying Bi content on the temperature-dependent mechanical, dielectric, and structural properties of nominal $Na_{1/2}Bi_{1/2}TiO_3$

Cite as: J. Appl. Phys. **130**, 185106 (2021); https://doi.org/10.1063/5.0070594
Submitted: 08 September 2021 • Accepted: 21 October 2021 • Published Online: 09 November 2021

Ahmed Gadelmawla, Kevin Riess, Johannes Birkenstock, et al.

AIP Publishing

Journal of Applied Physics ARTICLE scitation.org/journal/jap

Effect of varying Bi content on the temperature-dependent mechanical, dielectric, and structural properties of nominal $Na_{1/2}Bi_{1/2}TiO_3$

Cite as: J. Appl. Phys. **130**, 185106 (2021); doi: 10.1063/5.0070594
Submitted: 8 September 2021 · Accepted: 21 October 2021 ·
Published Online: 9 November 2021

Ahmed Gadelmawla,[1,a)] Kevin Riess,[1] Johannes Birkenstock,[2] Manuel Hinterstein,[3] Kyle G. Webber,[1] and Neamul H. Khansur[1,a)]

AFFILIATIONS

[1]Department of Materials Science and Engineering, Friedrich-Alexander-Universität Erlangen-Nürnberg (FAU), Martensstraße 5, 91508 Erlangen, Germany
[2]Fachbereich Geowissenschaften, Universität Bremen, Klagenfurter Straße 2-4, D-28359 Bremen, Germany
[3]Karlsruher Institut für Technologie, Institut für Angewandte Materialien, 76131 Karlsruhe, Germany

[a)]**Authors to whom correspondence should be addressed:** ahmed.gadelmawla@fau.de and neamul.khansur@fau.de

ABSTRACT

$Na_{1/2}Bi_{1/2}TiO_3$ (NBT) with varying Bi content has gained significant interest as a potential new material for solid-oxide fuel cells and oxygen separation membranes because of its excellent oxygen-ion conductivity. In this work, the effect of varying Bi content in NBT ceramics of compositions $Na_{1/2}Bi_xTiO_{2.25+1.5x}$, where $x = 0.485$–0.510, on the temperature-dependent mechanical and dielectric properties and the crystal structure has been investigated, as these applications expose the components to high thermal and mechanical fields. The effects of Bi variation on phase compositions and structural transitions were systematically investigated by scanning electron microscopy-energy dispersive x-ray analyses and neutron diffraction at room temperature, *in situ* high-temperature x-ray diffraction, dielectric permittivity, and mechanical measurements. In-depth analysis of the temperature-dependent data shows that the Bi content of the samples does not alter the average crystal structure of the NBT; however, the temperature-dependent behavior of the latter depend on variations in Bi content and the associated oxygen vacancy concentration. This change in phase transition temperature displays a good correlation with the temperature-dependent ferroelastic response and with the Bi content.

I. INTRODUCTION

The perovskite sodium bismuth titanate $Na_{1/2}Bi_{1/2}TiO_3$ (NBT) is one of the key components of a number of interesting piezoelectric ceramic compositions with technological importance. For example, NBT-based solid solutions with other perovskites, such as $BaTiO_3$, $Bi_{1/2}K_{1/2}TiO_3$, $CaZrO_3$, and $SrTiO_3$, are extensively investigated for the electromechanical applications, such as high-stroke actuators and high temperature (>300 °C) stable dielectric capacitors.[1–7] The origin of such interesting properties is considered to be related to the existence of structural and compositional disorder in the NBT-based solid solutions.[8–12] Interestingly, although pure NBT is considered to be a relaxor in the as-processed state, the structural, microstructural, and electromechanical properties are not similar to classical relaxor or ferroelectric materials.[13]

Although NBT was first reported in 1961 by Smolenskii *et al.*,[14] the room-temperature crystal structure and the existence of relaxor ferroelectric characteristics are still debated. The room temperature crystal structure of NBT was originally reported to have space group symmetry *R*3*c*.[15] Later works have demonstrated that the crystal structure of NBT is more complex with nano-scale variation.[8,10,16–20] For example, microstructural investigation using transmission electron microscopy showed the existence of nanosized domains within the bulk matrix.[21] As such, NBT exhibits unique and interesting phase transitions, phase coexistence, and domain structure as well as structural disorder and oxygen octahedral tilting associated with anisotropic diffuse scattering.[19,22] One of the possible reasons for such structural variation is closely related to the coexistence of different polar displacements of the Bi^{3+} cations.[16] Moreover,

experimental diffuse scattering data from single crystal NBT were modeled using correlated A-site occupation and the atomic size effect.[23] The local scale variation makes it challenging to investigate the crystal structure using diffraction methods. Beanland and Thomas[24] showed using TEM investigation of single crystal that the defect free region of NBT is indeed rhombohedral with space group *R*3*c*. This report implies that although individual unit cells may have Bi^{3+} displacement which are not along $[111]_{pc}$, the average bulk symmetry of NBT is rhombohedral, *R*3*c*. Nevertheless, the average crystal structure of NBT can be sufficiently modeled using *R*3*c*.[24–26]

The volatilization of Bi and Na oxides in NBT is often unavoidable during the solid-state processing due to calcination and densification at elevated temperatures.[27–29] Generally, excess amounts of constituent powders are added to compensate for the potential loss during the sintering process. Importantly, Li *et al.*[30] showed a significant influence of A-site occupation factor on the electrical conductivity and oxygen ion conduction mechanisms, demonstrating that NBT with varying Bi content might be interesting as an electrolyte material with a fast oxygen ion conduction for intermediate temperature solid oxide fuel cells (SOFCs).[31] Recent works have demonstrated that the predominantly ionic conducting character can be established in NBT with a slight variation in A-site occupanices.[29,32] The Bi/Na ratio plays a crucial role in determining the electrical behaviors, i.e., Bi/Na > 1 favors insulating properties at room temperature, whereas Bi/Na ≤ 1 exhibits high oxygen ion conductivity.[33] Additionally, A-site deficiency has been found to influence the cationic diffusion kinetics during the solid-state processing, for example, diffusion rate of Sr^{2+} in $Na_{1/2}Bi_xTiO_3$-$SrTiO_3$ compositions is significantly different depending on the Bi deficiency or excess in the sample, where faster grain boundary diffusion was used to produce core–shell structures.[2] As such, A-site deficiency plays a crucial role in the observed functional properties in NBT.

Analogous to an applied electric field, mechanical stress can influence the crystal structure, long-range ordering, and domain orientation.[34–36] For example, it has been demonstrated that long-range ferroelectric order can be established in NBT-based relaxor ferroelectrics using mechanical stress.[37–39] As such, the macroscopic electromechanical properties and the temperature stability can be influenced by the externally applied mechanical stress,[40] making the investigation of the influence of mechanical stress critical, as functional ceramics often experience both elevated temperatures and significant mechanical stresses during both processing and operation. For example, coefficient of thermal expansion mismatches between the cathode, anode, electrolyte, and interconnect in an SOFC can lead to elevated internal residual stresses that causes component degradation and eventual failure.[41–43] Despite this, the temperature-dependent crystal structure and mechanical properties as a function of varying Bi content have not been investigated in detail. As such, the influence of varying Bi content on the average crystal structure of the NBT ceramics from room temperature to 560 °C was investigated and correlated to the temperature-dependent data on ferroelasticity and on the dielectric response in this work.

II. EXPERIMENTAL METHODOLOGY

$Na_{1/2}Bi_xTiO_{2.25+1.5x}$ (NB_xT) ceramic compositions with varying Bi content of 0.485, 0.490, 0.500, and 0.510 were prepared using the conventional solid-state route. Na_2CO_3 (99.50%, Alfa Aesar, Germany), Bi_2O_3 (99.99%, Projector, Germany), and TiO_2 (99.60%, Alfa Aesar, Germany) were used as the starting materials. All starting materials were kept at 120 °C for at least 24 h to minimize the influence of the atmospheric moisture content. The required amounts of constituent raw materials were weighed in a glovebox with reduced (<12%) humidity. Following weighing, powders were milled and mixed for 24 h in a rolling mill using ethanol and zirconia milling balls (5 mm); the resulting ceramic slurry was then dried using a rotary evaporator. A two-step temperature profile at 700 and 800 °C with a dwell time of 2 and 3 h, respectively, was used for calcination.[30] A second milling step of calcinated powder was conducted to improve the particle size homogeneity. Cylindrical samples were prepared by uniaxial pressing and cold isostatically compacted with a pressure of 180 MPa. The green bodies were sintered at 1150 °C for 2 h in air with a heating and cooling rate of 5 K/min. For mechanical measurements, samples with a height of 6.00 (±0.01) mm and a diameter of 5.80 (±0.01) mm were prepared by surface grinding and lathing. Pt electrodes were sputtered on the cylindrical faces for dielectric measurements. Prior to the mechanical and electrical measurements, samples were annealed at 600 °C for 2 h with a heating rate of 5 K/min and a cooling rate of 1 K/min to remove residual stresses that the sample preparation steps might induce.

Microstructure, element distributions, and phase fractions were analyzed using scanning electron microscopy (SEM) (Helios NanoLab 600i FIB Workstation, FEI Company, OR, USA) equipped with energy dispersive x-ray (EDX) and electron backscatter diffraction (EBSD) detectors (Oxford Instruments NanoAnalysis, Wiesbaden, Germany). The respective samples were polished with a 1 μm diamond suspension followed by a final treatment with an oxide-polishing suspension. Grain size analysis was performed using ImageJ software[44] on three images of respective samples, where at least 100 grains were measured. The chemical analysis of the four sintered samples was performed using inductively coupled plasma optical emission spectroscopy (ICP-OES) (Spectro Genesis, Spectro Analytical Instruments GmbH, Germany).

A custom-built setup equipped with an LCR meter (E4980AL, Keysight, USA) and a furnace (LE4/11/3216, Nabertherm, Germany) was used to determine the temperature-dependent dielectric permittivity and dielectric loss from room temperature to 600 °C in the measurement frequency range of 1 kHz to 1 MHz.

Macroscopic temperature-dependent mechanical measurements up to 400 °C were carried out with a screw-type load frame (Zwick/Roell Z030, Zwick GmbH & Co. KG, Germany) equipped with a thermal chamber. The load was controlled by a 30 kN load cell, whereas the sample's displacement was measured with a custom-build linear variable differential transformer system. Detailed descriptions of the experimental arrangement can be found elsewhere.[45] For each composition, uniaxial compressive tests were performed in the temperature range from room temperature to 400 °C with a step size of 25 °C. The temperature was kept constant before the measurement until the temperature fluctuation was less than ±0.1 °C of the setpoint value. To maintain the contact between the sample and the load bearings during heating, an initial pre-load of −3.8 MPa was applied. Subsequently, the samples were loaded to a maximum stress of −500 MPa with a rate of 5 MPa/s and unloaded with the same rate. The relative errors in the evaluated ferroelastic

parameters were estimated by means of the standard deviation of five measurements at room temperature of the representative compositions and then the percentage was applied over the entire temperature range, taking into consideration that the error is due to minor misalignment of the sample and hence independent of the temperature.

Neutron diffraction was performed at the Wombat beamline at the Australian Nuclear Science and Technology Organization (ANSTO) in Sydney, Australia.[46] Diffraction patterns of the ceramic powder were collected by means of a curved position sensitive detector using monochromatic radiation with a wavelength of $\lambda = 1.63$ Å. Temperature-dependent changes in the phases of both the powder and sintered bulk NBT samples were investigated using a powder diffractometer (Bruker D8 Discover, Bruker GmbH, Germany) equipped with a Cu tube. The step size was 0.010° and 57.6 s/step, scanning range 20°–100° with fixed divergence slit 0.26°, primary and secondary Soller slits of 2.5°, and a total detector PSD aperture of 3.296° 2θ in 192 channels (~0.0171° 2θ per channel). A corundum sample holder with a blind hole of 0.8 mm depth and a diameter of 16 mm was used in a heating chamber (Anton Paar HTK1200, Anton Paar Germany GmbH, Germany) for high-temperature measurements within a range from 27 °C (room temperature) up to 560 °C. Before each measurement, the temperature was equilibrated for at least 15 min.

Full pattern structural refinements of all the diffraction data were conducted using software package TOPAS v.5.[47] The instrumental peak shapes for XRD data were optimized with respect to LaB_6 data using the fundamental parameter approach in TOPAS. In the case of neutron powder diffraction (NPD) data, the instrument profile was refined based on Al_2O_3 powder with Pseudo-Voigt Function. For the combined structural refinement of XRD and NPD data of powder samples, the lattice parameters (a, b, c) were refined based on XRD data, whereas the atomic positions (x, y, z) and displacement parameters (B) were based on NPD data. The O_z position was kept fixed to 1/12 for all refinements after Megaw and Darlington[48] to fix the origin (in $R3c$ the origin of the unit cell is not fixed in terms of z). The background was matched with Chebychev polynomial refinement. Beyond that phase-specific peak broadening parameters were refined to account for crystallite size and microstrain effects. For the temperature-dependent XRD data, in addition to the lattice parameters and atomic coordinates, sample displacement was refined for all steps for powder and bulk samples. However, some extra corundum peaks were observed for bulk samples from the XRD sample holder, which is offset by −0.8 mm compared to the sample surface. The resulting difference in the sample displacement and sample holder displacement was resolved by refining sample tilt in TOPAS.

III. RESULTS AND DISCUSSION

A. Microstructure and electromechanical properties

1. Microstructure and chemical compositions

Figures 1(a)–1(d) show representative microstructure images of NB_xT ceramics. As expected, the variable Bi content was found to have a profound influence on the microstructure, where increased Bi deficiency significantly increased the observed grain size. The samples with a nominal Bi excess ($NB_{0.510}T$) and a nominally stoichiometric composition ($NB_{0.500}T$) displayed grain sizes of 1.26 (± 0.62) μm and 1.65 (± 0.45) μm, respectively. In contrast, the samples with Bi deficiency showed large grains with a grain size of 14.20 (±3.52) μm and 11.83 (±2.11) μm for $NB_{0.490}T$ and $NB_{0.485}T$, respectively. These observations are consistent with previous reports.[28,49] The increased grain growth of the Bi-deficient compositions, i.e., $NB_{0.490}T$ and $NB_{0.485}T$, can be attributed to the enhanced surface diffusion mechanisms due to the higher oxygen deficiencies in these samples, which are understood to be primarily responsible for coarsening during densification. Similar effects were shown for Mg-doped NBT, where acceptor doping resulted in enhanced diffusion and significant grain growth.[50] It is evident that pores occur within large grains [Figs. 1(a) and 1(b)], whereas in compositions with a smaller grain size these are mostly located at the grain boundaries [Figs. 1(c) and 1(d)]. The enclosed pores within the grains indicate the higher grain boundary mobility than the pore mobility in the Bi-deficient compositions during the sintering process.[51,52] In addition, the $NB_{0.510}T$ sample exhibits precipitates at the triple junctions, evident as bright areas, which were found through EDX analysis to be a Bi-rich phase (Bi_2O_3). Assuming that all Bi exceeding ½ atoms per formula would go into the second phase, we could expect ~1 mol. % Bi_2O_3 phase in the sample supports the data presented in Fig. 1(d). Similar observations have been reported in the literature for this composition.[53] Nevertheless, the EDX analysis shows a homogenous distribution of the elements in the samples, accordingly, missing the minor second phase Bi_2O_3, possibly due to limited spatial resolution. The phase compositions were observed by EBSD and analyzed with Oxford Instruments HKL Technology CHANNEL 5 software package. The data acquisition with an accelerating voltage of 20 keV and a step size of 0.117 μm confirmed a single phase of rhombohedral structure at room temperature for all samples (see supplementary material), meaning again that the minor Bi_2O_3 phase is not detected. This is likely due to the small amount of the Bi_2O_3 phase. The ICP-OES analysis showed that the Bi content ratio was 0.479, 0.486, 0.489, and 0.498 for $NB_{0.485}T$, $NB_{0.490}T$, $NB_{0.500}T$, and $NB_{0.510}T$, respectively. Within the measurement accuracy of the ICP-OES, it can be stated that the $NB_{0.510}T$ composition is closer to the nominally stoichiometric NBT. For all samples, the actual composition differs from the nominal one, exhibiting smaller Bi content in the actual analyses. For further discussions, we keep the nominal compositions for sample notation, but it should be kept in mind that none of the samples exhibited excess Bi, yet there is a distinct series of Bi content ranging from 0.479 to 0.498 Bi atoms per formula unit. As such, although there is no sample with actual excess Bi after long-term heat treatment and densification process, the chemical and microstructure investigation of the studied compositions confirms that there is a pronounced influence of varying Bi content on the microstructure of NBT-based ceramics in NBT-based compositions.

2. Temperature-dependent dielectric properties

The stoichiometry and the grain size are known to have a significant impact on the dielectric properties of perovskite ferroelectrics.[54] As such, the temperature-dependent dielectric permittivity

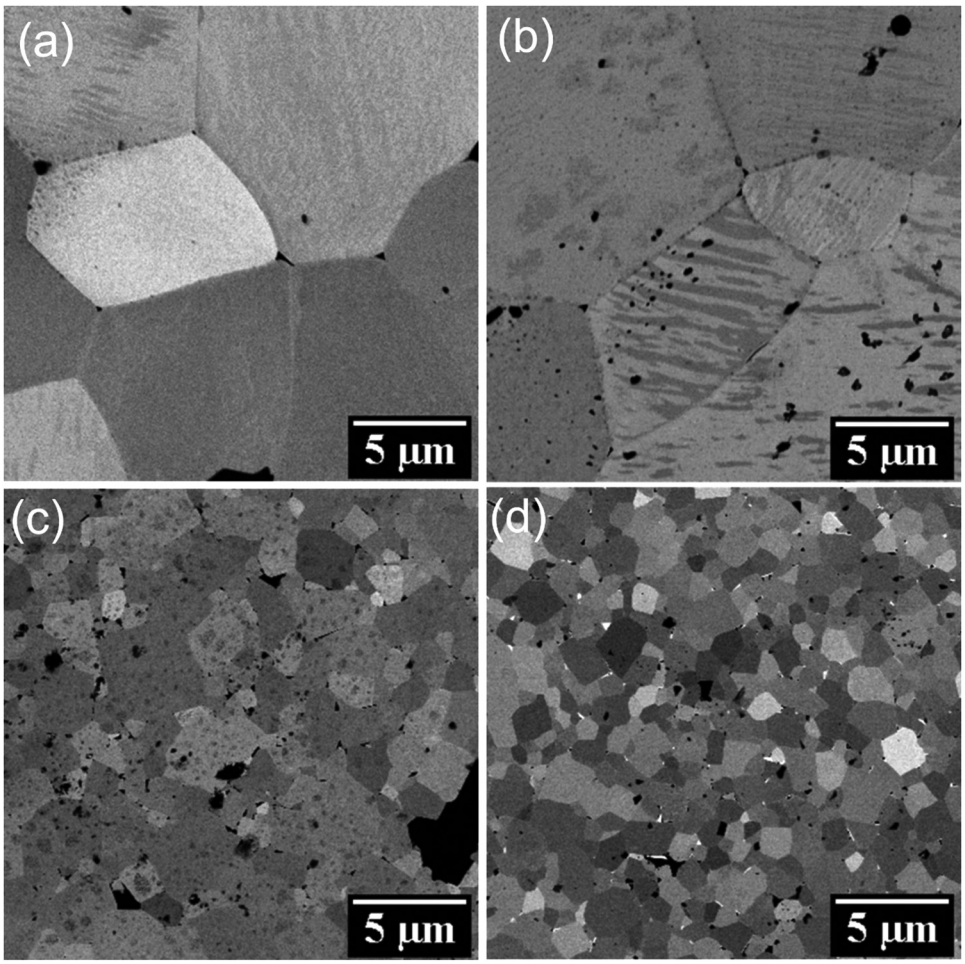

FIG. 1. Surface microstructure images of samples with different Bi content: (a) $NB_{0.485}T$, (b) $NB_{0.490}T$, (c) $NB_{0.500}T$, and (d) $NB_{0.510}T$.

and dielectric loss data were characterized from room temperature to 600 °C for unpoled polycrystalline NB_xT with varying Bi content, as shown in Figs. 2(a)–2(d). At room temperature, increasing Bi content was found to decrease the extent of frequency-dependent dispersion in dielectric loss, consequently resulting in the macroscopic response of the $NB_{0.510}T$ composition resembling a stoichiometric NBT,[55] which is supported by the ICP-OES analysis. Nevertheless, the dielectric permittivity response as a function of Bi content differs significantly with increasing temperature. It is apparent that a decreasing Bi content significantly increases the dielectric loss at elevated temperatures, in particular, for lower frequencies, which is suggested to be due to an increased structural defect concentration. At the highest frequency (1 MHz), all compositions show a similar temperature-dependent characteristic of the dielectric response, consistent with previous investigations.[28,49] With increasing temperature, a shoulder at ∼200 °C followed by a sharp increase in the relative permittivity in the range of 300 °C can be detected for all compositions, although this effect is most pronounced in $NB_{0.510}T$. With increasing Bi content, the temperature of the maximum slope of the permittivity, defined here as T_{R-T} in the following discussion,[56,57] shifts toward higher temperatures from 295 to 304 °C. With further increasing temperature, the relative permittivity merges into a broad maximum T_m, which is also shifted to higher temperatures from 318 to 326 °C with increasing Bi content, corresponding with a diffuse minimum in the dielectric loss. Above T_m the permittivity initially decreases, whereas the loss increases, which can be attributed to the increased oxygen-ion conductivity.[29]

Considering the stoichiometric starting composition $NB_{0.500}T$, the oxygen-ion conductivity is understood to be a consequence of the Bi evaporation during sintering, whereas for $NB_{0.485}T$ and $NB_{0.490}T$ the conductivity is due to both the Bi evaporation and the Bi deficiency of the starting composition. At low frequencies, the influence of conductivity on the dielectric response is more pronounced as charge carriers are given more time to move. Nevertheless, the temperature-dependent permittivity behavior of $NB_{0.510}T$ indicates that the nominal Bi-excess composition is electrically insulating at room temperature, i.e., insulating nature is predominant over the oxygen-ion conducting behavior.[29]

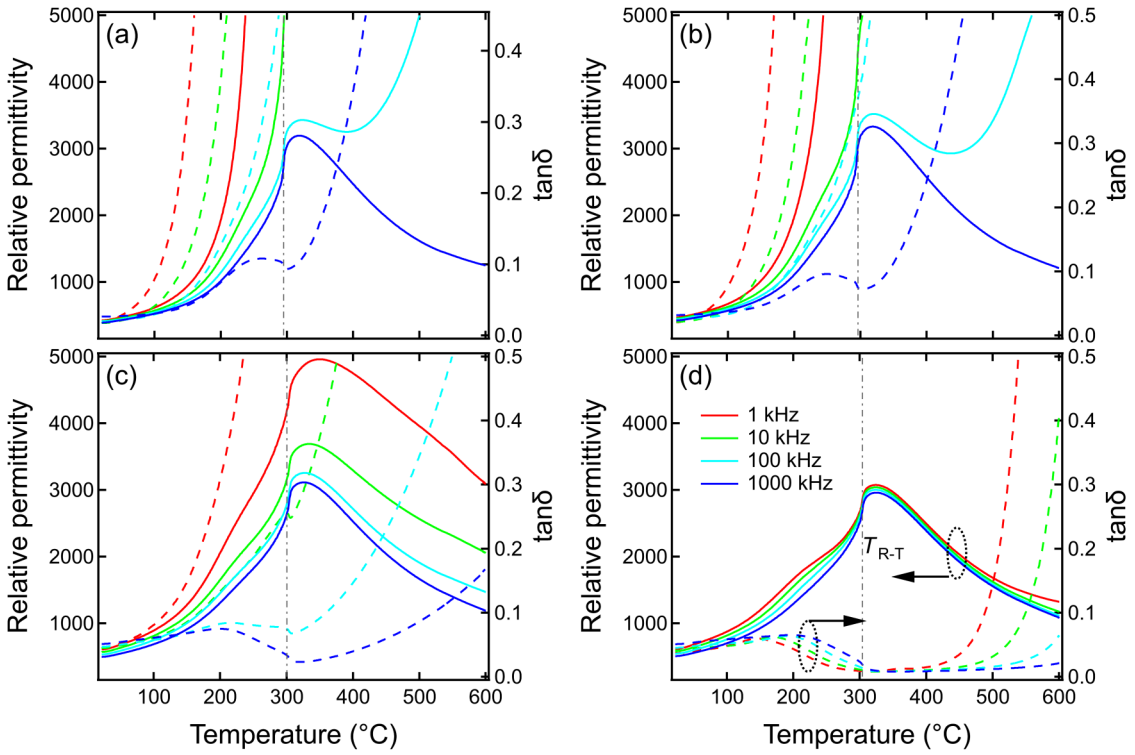

FIG. 2. Temperature-dependent dielectric permittivity (solid lines) and tan δ (dashed lines) as a function of Bi content; (a) $NB_{0.485}T$, (b) $NB_{0.490}T$, (c) $NB_{0.500}T$, and (d) $NB_{0.510}T$.

3. Temperature-dependent ferroelasticity

Mechanical measurements were used to investigate the large-field electromechanical response of NBT samples with varying Bi content, as the increased conductivity observed in Bi-deficient compositions precluded large-field electrical measurements, especially at elevated temperatures. The temperature-dependent macroscopic constitutive mechanical behavior was characterized for all four compositions from 22 to 400 °C, where a ferroelastic response was marked by a non-linear stress–strain behavior and the formation of a hysteresis with corresponding coercive stress, strain saturation, and remanent strain. Figure 3 shows the temperature-dependent stress–strain behavior at representative temperatures for all compositions, which displayed ferroelasticity over the whole temperature range. The ferroelastic response can be described by several characteristic parameters, such as onset σ_o (estimated by tangent intersection method)[40] and coercive stress σ_c (the inflection point during loading),[40] which indicate the initiation of ferroelastic reorientation through the nucleation and growth of domain walls and the maximum rate of domain switching during the loading, respectively,[40] as well as the remanent strain ϵ_r, representing the strain remaining following mechanical unloading. With a further increase in stress above σ_c, the mechanical response becomes approximately linear again up to the maximum stress due to the saturation of the switching process. During unloading, the material response is initially linear but deviates from linearity due to the influence of local electrical and mechanical fields causing the domains to return to their original orientations, denoted as backswitching.[13]

Temperature-dependent variations in the crystal structure and domain wall mobility result in changes in both the coercive stress and remanent strain with increasing temperature, as shown for all compositions in Fig. 4. At room temperature, σ_c displayed an apparent decrease with increasing Bi content from above the measurement range of −500 MPa for $NB_{0.485}T$ to −426 (±11) MPa for $NB_{0.500}T$. This corresponded with a decrease in remanent strain from −0.156 (±0.019) % to −0.081 (±0.009) % for $NB_{0.500}T$ and $NB_{0.485}T$, respectively. The composition-dependent variation in room-temperature coercive stress and remanent strain can be related to the defect concentrations associated with the change in Bi content, such as pores or oxygen vacancies, which can hinder domain wall motion.[40]

With increasing temperature to 100 °C, there is a reduction in the coercive stress by approximately 50%, resulting in an increase in the remanent strain for all compositions that is due to an enhanced mechanical saturation. Above this temperature, however, both the coercive stress and remanent strain decrease, with the coercive stress values for all compositions converging at temperatures above 150 °C, making them independent of Bi content. Similar effects have been observed in other ferroelectric and ferroelastic materials, which was attributed to the reduced spontaneous

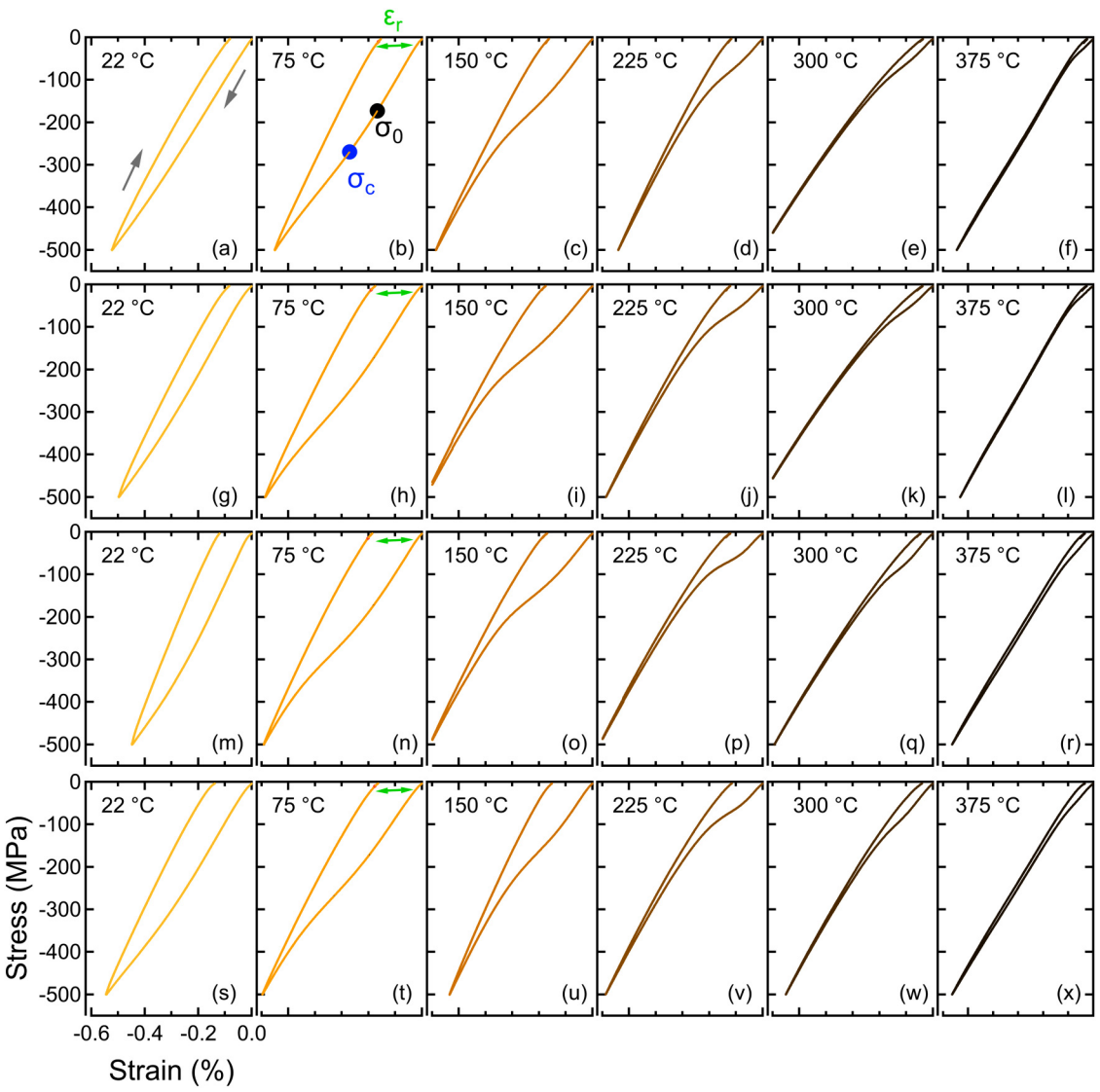

FIG. 3. Representative temperature-dependent stress–strain behavior of [(a)–(f)] $NB_{0.485}T$, [(g)–(l)] $NB_{0.490}T$, [(m)–(r)] $NB_{0.500}T$, and [(s)–(x)] $NB_{0.510}T$ at from 22 to 375 °C.

strain of the unit cell with increasing temperature.[58,59] Interestingly, around 300 °C, i.e., at the R-T phase transition,[60,61] the coercive stress values display a Bi content independent anomaly, whereby the coercive stress increases from approximately −50 to −100 MPa, followed by a decreasing trend with further increasing temperature. This same anomaly is not observed in the remanent strain, where a saturation above 275 °C is observed up to 400 °C, indicating that stress-induced hysteretic processes are retained. It was observed that the hysteresis decreases with temperature and above approximately 200 °C this becomes insensitive to the Bi content (Fig. 3). It is also important to note that the variation in coercive stress and remanent strain can also be related to the Bi content-dependent differences in the grain size (Sec. III A 1). Previous works have demonstrated that grain size can have a significant effect on the dielectric[54] and ferroelectric[62,63] response of perovskite ferroelectrics, which is understood to be primarily due to changes in the extrinsic contributions, e.g., domain wall nucleation and growth. In contrast, however, previously reported microstructural effects on the mechanical properties of PZT revealed an increase in the coercive stress with decreasing grain size.[63] In the present work, an increase in the coercive stress was observed despite a grain size increase of nearly an order of magnitude, strongly indicating that the enhanced defect concentration in Bi-deficient compositions played an important role.

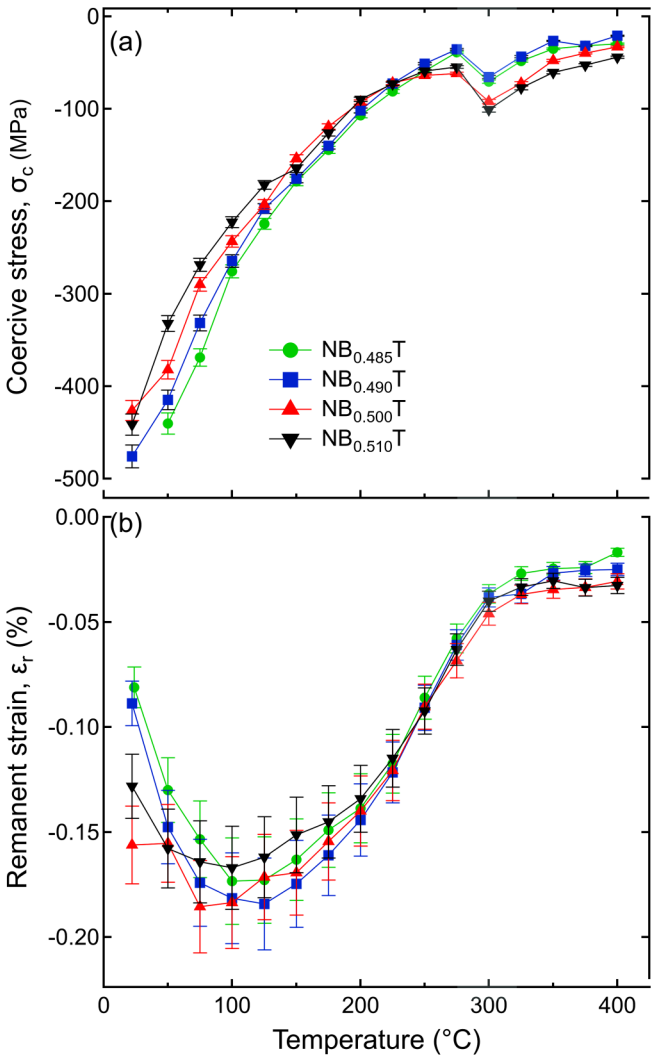

FIG. 4. Variation in temperature-dependent (a) coercive stress and (b) remanent strain as a function of Bi content.

B. Dependence of crystal structure parameters on Bi content

1. Influence of Bi content on crystal structure parameters at room temperature

X-ray and neutron diffraction patterns of all four NB_xT ceramic powders were collected at room temperature. The diffraction patterns revealed typical reflections of perovskite-type structures without any reflections of secondary crystalline phases within the resolution limit of the instrument used here. The variation in the crystal structure as a function of Bi content was determined using a combined Rietveld refinement of the x-ray and neutron diffraction patterns, which is beneficial because of the variation of scattering contributions of Bi^{3+}, Na^{+}, and O^{2-} in x-ray and neutron data. The neutron diffraction data can more reliably describe the oxygen positions and occupancies next to heavy ions such as Bi^{3+}.

The crystallographic data from the combined refinement of room temperature neutron diffraction and x-ray diffraction analysis for NB_xT with different Bi/Na ratios at room temperature are shown in Table I. Representative refined and observed profiles based on the rhombohedral structure model (space group *R3c*) are shown in Fig. 5 for powder $NB_{0.500}T$ XRD and NPD data. With changing Bi/Na ratio, the crystallographic data do not show a significant change in the lattice parameters; however, the changes in the tilt angle (ω) and octahedral strain (ξ) are significant. For the rhombohedral unit cell, *s*, *t*, *d*, and *e* are the distortion parameters that can be calculated from the refined atomic coordinates, where $Na/Bi_z = 1/4 + s$, $Ti_z = t$, $O_x = 1/6–2e–2d$, $O_y = 1/3–4d$.[48] These parameters represent the deviation in the atomic coordinates from its original position. From these distortion parameters, tilt angle (ω) and octahedral strain (ξ) can be calculated as follows:[48]

$$\tan\omega = 4 \times \sqrt{3} \times e,$$

$$\xi = \cos\omega\left(\frac{c_H}{a_H \times \sqrt{6}}\right)\text{-}1.$$

The displacement of Ti^{4+} along the *c* axis (*t*) shows a strong correlation with the Bi/Na ratio, where composition with Bi^{3+} deficiency exhibits a shifting of Ti^{4+} in the negative direction along the *c* axis and excess Bi^{3+} leads to a shift in the positive direction along the *c* axis. Atomic positions and lattice parameters were used to calculate the octahedral tilt angle ω, octahedral strain ξ, and the spontaneous polarization P_s. The evaluation of P_s along the hexagonal *c*-axis was conducted according to the equation reported by Frantti *et al.*[65] The calculated P_s [Table I(a)] varies between ~9.4 and ~16 $\mu C/cm^2$ depending on the Bi content, i.e., P_s increases with increasing Bi content. In fact, the P_s of $NB_{0.51}T$ composition matches well with the P_s of ~18.64 $\mu C/cm^2$ estimated using structural data reported in Jones and Thomas[66] for $NB_{0.500}T$ single crystal. Importantly, the major difference between the $NB_{0.500}T$ and other compositions NB_xT lies in the tilt angles ω, in addition to some extent in the octahedral strain. The nominal $NB_{0.510}T$ sample composition also shows smaller displacement parameters *B* compared to Bi-deficient and nominally stoichiometric compositions. This can at best be understood by the observation that the nominal $NB_{0.510}T$ sample contains a minor secondary phase Bi_2O_3 and thus the NBT ceramic here are probably closest to the composition $NB_{0.500}T$ with all crystallographic sites fully occupied. In conjunction with the above reported ICP-OES results, it can be concluded that most probably some of Bi evaporated from all samples during high temperature processing so that the actual compositions have all shifted to slightly lower Bi content on heat treatment.

2. Temperature-dependent variation in phase compositions and crystal-structure related parameters

The temperature-dependent XRD data in the range of 27–560 °C for powder and bulk (e.g., $NB_{0.510}T$) are shown in Fig. 6, where the crystal structure parameters show clear variation with increasing temperature. Qualitative observation indicates that upon

TABLE I. (a) Crystallographic data and derived quantities for NB_xT with different nominal Bi/Na ratios at room temperature and (b) atomic sites parameters.[a]

(a)				
Bi/Na	0.485/0.500	0.490/0.500	0.500/0.500	0.510/0.500
Space group		*R3c*		
Displacements		Along $[\mathbf{111}]_{\mathbf{pc}}$		
Tilt system[64]		$a^-a^-a^-$		
a_H (Å)	5.492(8)	5.492(9)	5.493(8)	5.492(9)
c_H (Å)	13.450(2)	13.448(2)	13.440(2)	13.44(2)
Volume (Å^3)	351.30(11)	351.24(12)	351.15(11)	351.18(13)
Density (g/cm^3)	5.88	5.92	5.93	5.97
s	0.0144	0.0136	0.0150	0.0156
t	−0.000 61	−0.000 39	0.000 56	0.003 01
e	0.0126	0.0125	0.0133	0.012 44
d	−0.0026	−0.002 65	−0.0035	−0.0035
ω (deg)	5.003	4.96	5.02	4.92
$\xi \times 10^2$	−1.71	−1.29	−0.018	−0.25
P_s (μC/cm^2)	9.699(3)	9.434(5)	11.589(3)	15.911(4)
V_{pc} (Å^3)	58.550	58.546	58.521	58.526
R_{wp}	5.57	5.73	5.09	5.50

(b)				
Atoms	*x*	*y*	*z*	B_{eq}/Å^2[b]
0.485/0.500				
Bi/Na	0	0	0.2644(17)	2.9(2)
Ti	0	0	−0.0006(20)	0.22(15)
O	0.1467(17)	0.3440(3)	1/12	2.45(11)
0.490/0.500				
Bi/Na	0	0	0.2636(16)	2.7(3)
Ti	0	0	−0.0003(30)	0.38(18)
O	0.1469(16)	0.3440(30)	1/12	2.17(12)
0.500/0.500				
Bi/Na	0	0	0.265(2)	2.5(3)
Ti	0	0	0.0005(20)	0.2(2)
O	0.1471(14)	0.3475(30)	1/12	2.43(11)
0.510/0.500				
Bi/Na	0	0	0.2656(20)	3.3(4)
Ti	0	0	0.003(5)	0.27(15)
O	0.1488(20)	0.3474(40)	1/12	2.56(14)

[a]All refinements were carried out in space group *R3c* in hexagonal setting as a combination of XRD and NPD using TOPAS v5.
[b]Refers to displacement parameter *B*, where $B = 8\pi^2u^2$ is the Debye–Waller factor.

heating, the rhombohedral-tetragonal phase transition appears around 250 °C, whereas the cubic phase was observed above 500 °C, a result that is consistent with previous reports on $NB_{0.500}T$.[57,66] Importantly, these data show that the average structure of NBT with varying Bi content can be modeled with the *R3c* phase in both the powder and bulk. Recent investigations have revealed the role of the skin effect on diffraction analysis of the bulk sample surface in NBT-BT-based materials, which was shown to be due to oxygen vacancies.[53,67] Despite variations in the Bi content in this study, however, such significant differences were not observed throughout the investigated temperature range.

Rietveld refinement of selected temperature-dependent data (350 and 500 °C) is shown for both powder and bulk samples in Fig. 7. Note that additional reflections of corundum were observed due to the sample holder for bulk samples. Structural refinement revealed that the 100_{pc} and 200_{pc} reflections at $20° < 2\theta < 25°$ and $45° < 2\theta < 50°$, respectively, are less well matched than the other reflections, which could be a sign of defects/microstrain in the local structure, especially in the [100] direction. A single *R3c* phase was used for matching the data taken at lower and moderate temperatures via the Rietveld refinements for both the powder and bulk samples.[66] However, at lower temperatures below approximately 75 °C, the reflections in the bulk sample were rather poorly matched compared to those at higher temperatures, which is possibly related to the difference between the local and average structure at room temperature. It should be mentioned here that the

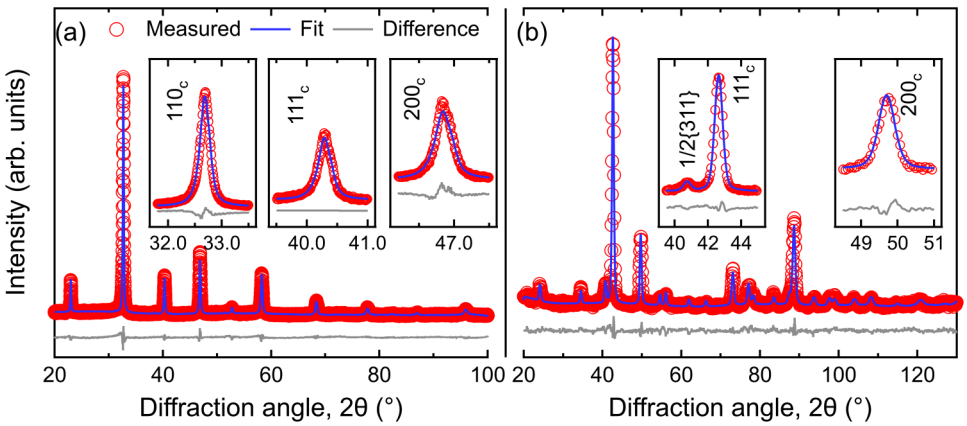

FIG. 5. Observed, calculated, and difference curves from the Rietveld refinement at room temperature with *R*3*c* for $NB_{0.500}T$ powder for (a) XRD and (b) NPD.

inclusion of the preferred orientation function did not improve the refinement quality of the bulk samples significantly. As such, it can be argued that the surface texture is possibly not the main cause of the poor fitting of the diffraction data of the bulk sample below 75 °C. The variation in local structure for NBT-based materials has been explained by the A-site occupancy and the atomic size effect.[23] More specifically, correlated displacements of Bi^{3+} and Na^{+} along the $<100>_{pc}$ directions have been found to be related to the observed diffuse scattering intensities for NBT single crystal. Nevertheless, it can be argued that with increasing temperature, the structural disorder becomes more dynamic and represents the average structure more accurately.

The tetragonal *P*4*bm* and the cubic $Pm\bar{3}m$ phases were used during refinement on data taken at high temperatures based on Jones and Thomas.[66,68] Within the temperature range of 300–350 °C, coexisting *R*3*c* and *P*4*bm* phases were used during the refinements, whereas at 500 °C the phases with symmetries *P*4*bm* and $Pm\bar{3}m$ were used. All samples were finally matched with the single cubic phase only at 560 °C (Fig. 7). The observed reflections shifted to lower 2θ upon heating due to thermal expansion. The 110_{pc} reflections in the range $30° < 2\theta < 35°$ were observed with an asymmetric shape and broadening, which can be due to the internal residual strain in the crystals resulting from distortion in the structure and anisotropic thermal expansion.

Using the temperature-dependent lattice parameters data, the thermal expansion slopes were calculated after linear fitting for all phases (Fig. 9). It was observed that the thermal expansion of unit cell volume increased with decreasing Bi content, where the $NB_{0.485}T$ displayed the highest volume expansion value of 2.48×10^{-3} Å^3/K, $NB_{0.490}T$ and $NB_{0.500}T$ showed the same expansion slopes with a value of 2.42×10^{-3} Å^3/K, and $NB_{0.510}T$ had a value of 2.40×10^{-3} Å^3/K. The changes in the temperature-

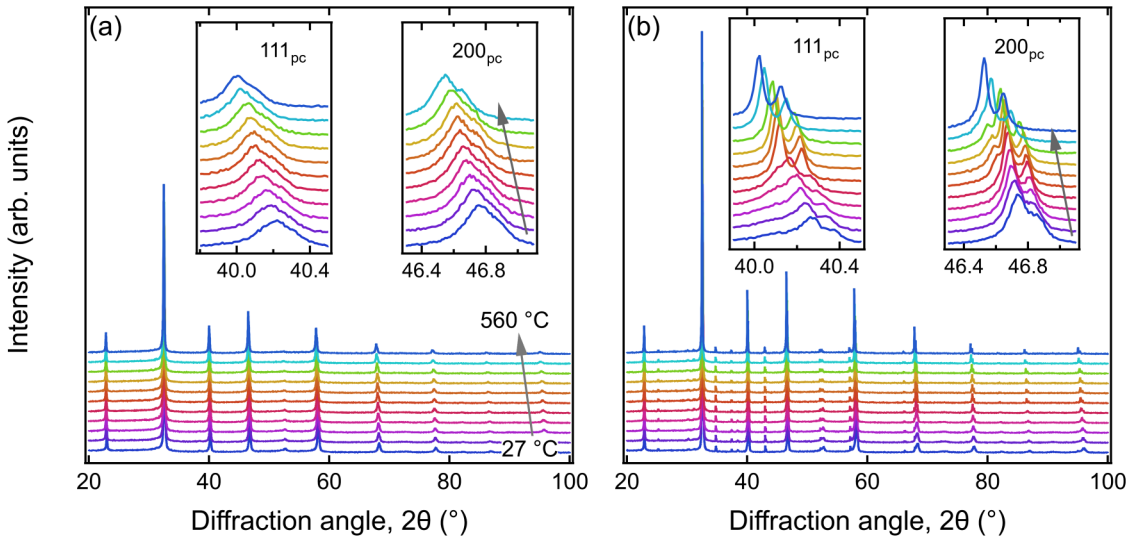

FIG. 6. Temperature-dependent XRD data of (a) powder and (b) bulk $NB_{0.51}T$ from 27 to 560 °C.

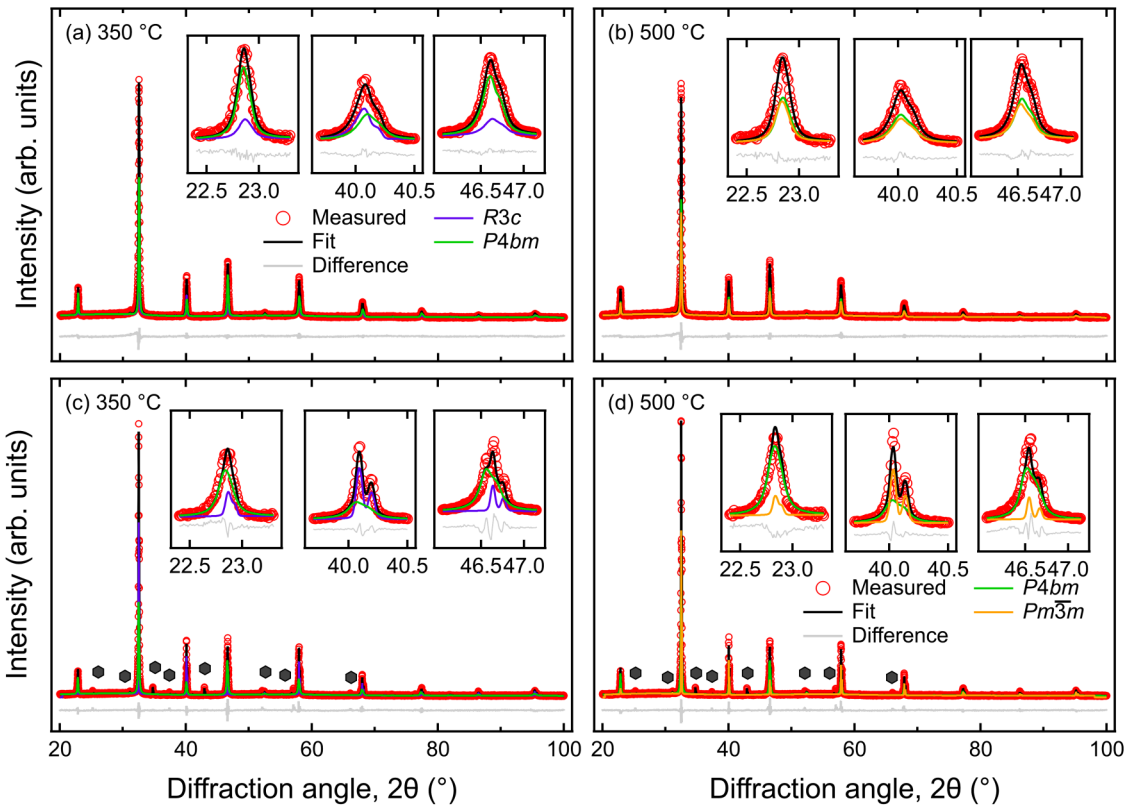

FIG. 7. High-temperature XRD data of powder [(a) and (b)] and bulk [(c) and (d)] $NB_{0.500}T$. The symbol ⬢ indicates the reflections from the corundum sample holder in the case of bulk samples.

dependent volume expansion coefficient are possibly related to the increased oxygen vacancy concentration associated with the reduced Bi content in the Bi-deficient materials, where the higher extent of oxygen vacancies allows the structure to expand relatively more than the compositions with a lower oxygen vacancy concentration.[69]

Rietveld refinement was performed for all temperature steps (Fig. 6), revealing the temperature-dependent variation in the phase fraction and unit cell volume, shown in Figs. 8 and 9. Importantly, the changes in the phase fractions were found to be slightly different for bulk and powder samples throughout the investigated temperature range, likely due to differences in internal stresses.[70,71] For example, the $NB_{0.485}T$ bulk sample at 300 °C displayed a phase content of approximately 64% rhombohedral and 36% tetragonal phases, whereas the phase content for the powder sample at the same temperature was 52% and 48%, respectively. Such variation in the phase fraction has previously been observed, for example, in KNN-based compositions, which has a well-known mixed phase orthorhombic–tetragonal region.[71] The ratio of tetragonal-to-rhombohedral phases increases with both increasing Bi/Na ratio and temperature up to 325 °C, corresponding well to previous investigations,[57] whereas the ratio of cubic-to-tetragonal phases decreases with increasing Bi/Na ratio (Fig. 8). However, within the error range of the temperature-dependent XRD data, there is no clear indication that Bi deficiency significantly alters the phase transition temperatures at the temperature resolution of our investigation. Moreover, the difference between rhombohedral and tetragonal volumes decreases in powder and bulk samples with increasing Bi/Na ratio, which can be a result of the decrease in oxygen deficiency with an increased amount of Bi.

The unit cell volume as a function of increasing temperature was determined, revealing the temperature-dependent volumetric thermal expansion coefficient of NBT with variations of Bi content (Fig. 9). A linear temperature-dependent change in unit cell volume for each separate phase is observed throughout the investigated temperature range. Interestingly, the rhombohedral–tetragonal phase transition in bulk samples displayed a clear jump in volume at approximately 300 °C, corresponding well with the sudden increase in coercive stress observed during mechanical measurements (Fig. 4). This might indicate the presence of a stress-induced tetragonal–rhombohedral phase transformation at 300 °C. A comparable jump in unit cell volume was not observed in the powder sample, suggesting that the internal mechanical and electrical fields present in the bulk sample played an important role.

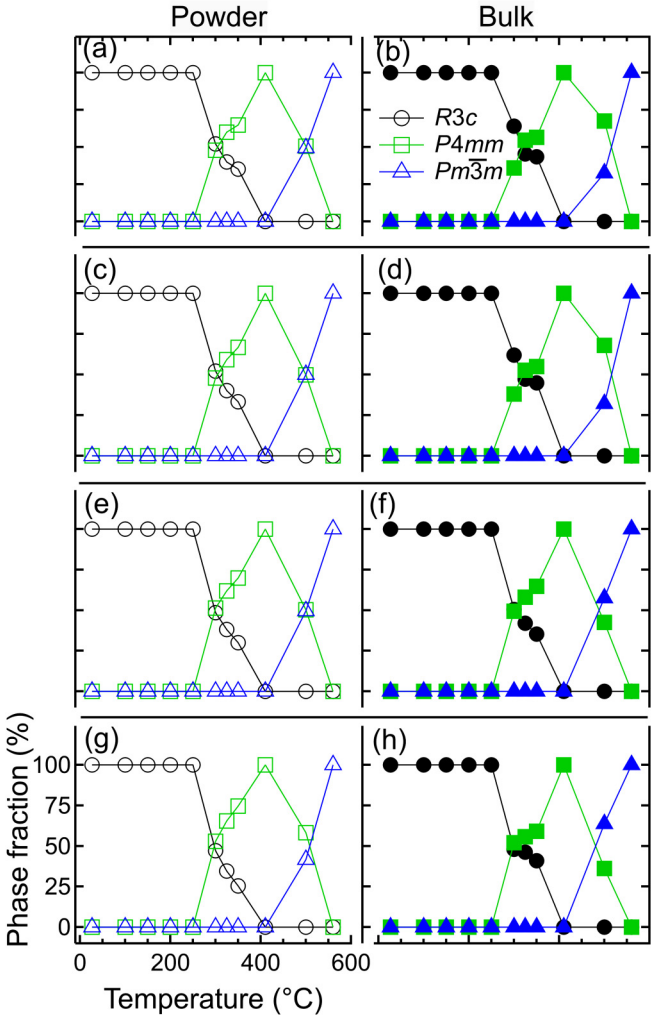

FIG. 8. Mass fractions of rhombohedral (black circles), tetragonal (green squares), and cubic (blue triangles) phases as a function of temperature for powder and bulk samples: [(a) and (b)] $NB_{0.485}T$, [(c) and (d)] $NB_{0.490}T$, [(e) and (f)] $NB_{0.500}T$, and [(g) and (h)] $NB_{0.510}T$. The phase fractions were determined after subtracting the corundum phase in bulk samples.

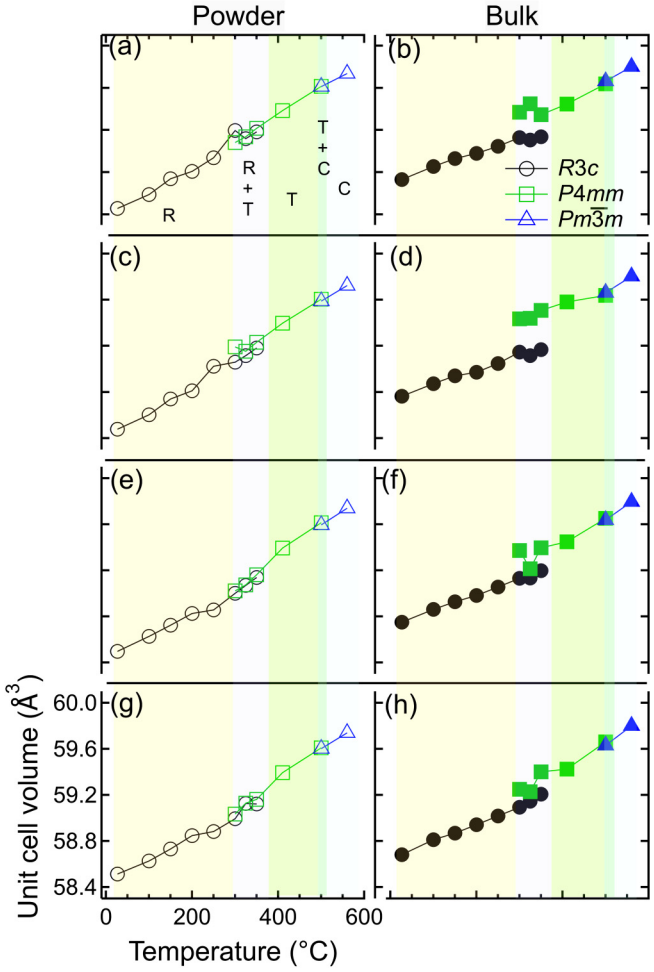

FIG. 9. Variation of unit cell volume as a function of temperature for powder and bulk $NB_{0.485}T$ [(a) and (b)], $NB_{0.490}T$ [(c) and (d)], $NB_{0.500}T$ [(e) and (f)], and [(g) and (h)] $NB_{0.510}T$.

Rhombohedral distortions (for $R3c$ space group, $\eta = \sqrt{2}c_{Rh}/2\sqrt{3}a_{Rh}$) and tilt angles in bulk samples were found to decrease upon heating until 250 °C, following which the distortion remained nearly constant upon further increasing temperature (Fig. 10). It should be mentioned here that the tilt angle and the lattice distortion are correlated.[48] Interestingly, although the phase fraction and unit cell volume (Figs. 8 and 9) of the respective bulk and powder compositions do not differ significantly with increasing temperature, the rhombohedral tilt angle and rhombohedral distortions show substantial differences. The bulk ceramic samples showed significantly higher tilt angle and lattice distortion than their powder counterpart. The anomaly in lattice distortion and tilt angle of the bulk samples around the 300 °C correlated well with the observed anomaly around 300 °C in temperature-dependent coercive stress and remanent strain (Fig. 4). The extent of lattice distortion plays a significant role in the extent of internal residual stresses in the polycrystalline ceramics,[72,73] i.e., the domain switching strain due to the field-induced non-180° domain switching process is also related to the unit cell distortion. As such, higher lattice distortion can increase the coercive stress and the extent of backswitching, reducing the remanent strain.

C. Influence of temperature-dependent crystal-structure parameters on dielectric and mechanical behavior

Previous investigations have shown that the dielectric shoulder at ~200 °C and the accompanied maximum in the dielectric loss,

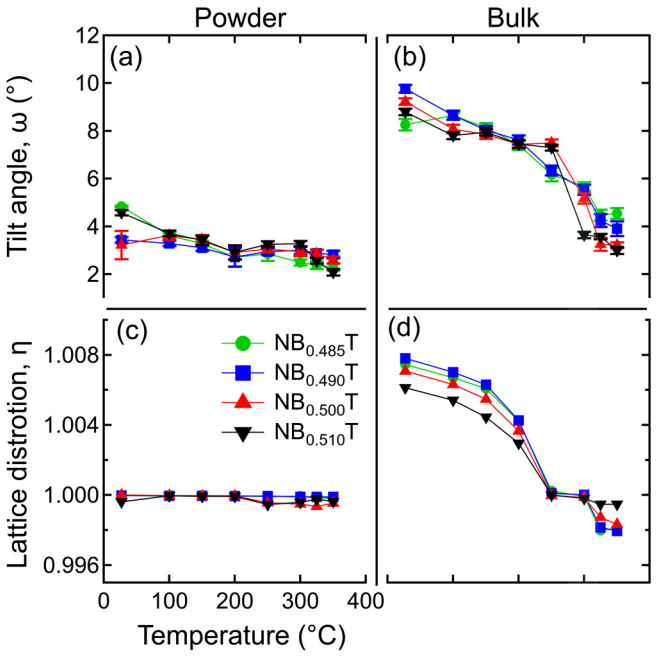

FIG. 10. Tilt angle ω and distortion η with 27–560 °C heating range; powder samples [(a) and (c)] and bulk samples [(b) and (d)].

both of which are particularly apparent in $NB_{0.510}T$, occur in the range of the rhombohedral (*R3c*) phase, which is stable up to ~250 °C. The anomaly is attributed to the decay of the ferroelectric state and in electrically poled NBT it was found to be more pronounced, where it marks the depolarization temperature.[74] In the cases of NB_xT, i.e., $x = 0.485$, 0.490, and 0.500, the shoulder around 200 °C is not prominent, possibly because of higher conductivity, especially at lower frequencies.[75] Between 250 and 400 °C, a broad coexisting region of rhombohedral and tetragonal (*P4bm*) phases is observed, where it was assumed that the corresponding transition temperature T_{R-T} coincides with the temperature at which the volume change between the two phases is the largest.[66] Interestingly, both T_{R-T} and T_m are shifted by 8 °C to lower temperatures due to a change in composition from the sample compositions with $NBi_{0.5}T$ or nominal Bi-excess ($NB_{0.500}T$ and $NB_{0.510}T$) to Bi-deficient compositions ($NB_{0.485}T$ and $NB_{0.490}T$). This may indicate a decreased phase transition temperature due to a reduced Bi content. However, such a shift in dielectric anomaly can be associated with conductivity.[75] In barium strontium titanate, a shift of the Curie temperature to lower temperatures by acceptor doping was demonstrated,[76] which was attributed to a local deformation (reduced distortion) due to the doping ions in combination with the formed oxygen vacancies. A similar effect is also possible in NB_xT, where the Bi deficiency gives rise to the formation of oxygen vacancies and the corresponding Bi vacancies increase the unit cell volume due to local cationic repulsion. This phenomenon has been observed previously in some mixed-conducting perovskite oxides in which the formation of oxygen vacancies leads to a thermochemical lattice expansion and the stability range of a phase can be shifted by several hundred degrees Celsius.[77] In addition, Suchanicz and Ptak[56] showed that the dielectric response of NBT is sensitive to compressive stress. A change in the unit cell volume and/or the distortion of the structure can also induce internal stresses and hence induce a shift of the characteristic temperatures. It should be noted that T_m is not accompanied by a discrete structural transition. With further increasing temperature, the permittivity decreases, despite the tetragonal phase stability up to 500 °C, followed by a narrow region of coexisting tetragonal and cubic phase up to a temperature of 540 °C. Above this temperature, the cubic phase is observed.

The variation in mechanical properties showed an overall decrease in the coercive stress with increasing temperature that can be attributed to a decreasing energy barrier for domain switching due to the increased thermal energy and the reduced crystal structure distortion [Fig. 10(d)].[59,78] In the vicinity of the coexisting range of rhombohedral and tetragonal phases, an increase in the coercive stress can be due to the interaction of the two phases, which was observed previously in lead-free perovskite ferroelectric materials, e.g., by means of an increased coercive field.[79] Martin *et al.*[80] showed a reversible transition in the orthorhombic-tetragonal phase transition region in $(Na_{0.5}K_{0.5})NbO_3$-based materials and a related increase in the coercive stress. The decrease in remanent strain with temperature can be explained by the reduced distortion of the unit cell with increasing temperature, corresponding well with η (Fig. 10).

At room temperature, the defect concentration determines the magnitude of the coercive stress and the remanent strain, e.g., acceptor doping can induce the formation of defect complexes comprising an oxygen vacancy and a dopant ion, which increase the critical ferroelectric/ferroelastic switching fields due to domain wall pinning[81–83] through, for example, clustering at domain walls.[84–86] Consequently, a reduced Bi content and accompanied higher oxygen vacancy concentration are understood to increase the coercive stress. In addition, the pores observed in the Bi-deficient compositions may further restrict domain wall nucleation and growth.[87] With increasing temperature, the influence of the defects on the coercive stress decreases due to the enhanced mobility of the oxygen vacancies and reduced coercive stress, initially increasing the remanent strain.[30] In the coexisting regime of rhombohedral and tetragonal phases, the magnitude of the coercive stress is reversed, and the Bi-deficient samples exhibit reduced values. Here, the grain size is likely the decisive factor; a small grain size induces internal stresses, which increase the coercive stress.[88]

IV. CONCLUSIONS

The temperature-dependent permittivity, ferroelastic properties, and crystal structure of NB_xT were investigated as a function of Bi content. ICP-OES data evidence that all samples presented had a slightly lower Bi content than the nominal compositions expected from synthesis, which is related to the vaporization of the constituent element during the high-temperature reaction and densification processes. Accordingly, none of the samples exhibited excess Bi content after sintering, yet still in the series from $NB_{0.485}T$ to $NB_{0.510}T$ increasing Bi content were confirmed ranging

from $NB_{0.479}T$ to $NB_{0.498}T$. The observation of minor second phase Bi_2O_3 in nominal composition $NB_{0.510}T$ with actual composition $NB_{0.498}T$ indicates that even in this sample the NBT phase is likely slightly Bi deficient. The comprehensive analysis of *in situ* high temperature XRD data indicates that the variation in Bi content does not significantly influence the temperature-dependent crystal structure and/or phase transition temperature. This suggests that the average *R3c* structure of NBT ceramics is not influenced by the variation in Bi content. However, the local structural analysis will be important to further highlight the influence of Bi deficiency. Nevertheless, our analysis showed that the temperature-dependent macroscopic ferroelastic response and the structural distortion are correlated. More specifically, the coercive stress and remanent strain as a function of temperature have a similar trend to the temperature-dependent rhombohedral distortion. The decrease in coercive stress with increasing temperature is associated with the decrease in lattice distortion as well as increased mobility of domain walls at higher temperatures. Additionally, the anomaly in the temperature-dependent ferroelastic response around 300 °C is suggested to be related to the change in phase fraction and unit cell volume change due to the rhombohedral–tetragonal phase transition.

SUPPLEMENTARY MATERIAL

See the supplementary material for elemental analysis of the compositions using Electron backscatter diffraction and energy-dispersive x-ray spectroscopy.

ACKNOWLEDGMENTS

The authors gratefully acknowledge the financial support for this work from the Deutsche Forschungsgemeinschaft under Grant Nos. GRK2495/H, WE 4972/5, and HI 1867/1-2. The authors would like to thank ANSTO for beamtime at the Wombat Beamline and Central Laboratory for Crystallography and Applied Materials Sciences at the University of Bremen for *in situ* HTK-XRD data collection.

AUTHOR DECLARATIONS

Conflict of Interest

The authors have no conflicts to disclose.

Author Contributions

A.G. and K.R. contributed equally to this work.

DATA AVAILABILITY

The data that support the findings of this study are available within the article and its supplementary material.

REFERENCES

[1]W. Jo, R. Dittmer, M. Acosta, J. Zang, C. Groh, E. Sapper, K. Wang, and J. Rödel, J. Electroceram. **29**, 71 (2012).
[2]T. Frömling, S. Steiner, A. Ayrikyan, D. Bremecker, M. Dürrschnabel, L. Molina-Luna, H.-J. Kleebe, H. Hutter, K. G. Webber, and M. Acosta, J. Mater. Chem. C **6**(4), 738–744 (2018).
[3]M. Höfling, S. Steiner, A.-P. Hoang, I.-T. Seo, and T. Frömling, J. Mater. Chem. C **6**(17), 4769–4776 (2018).
[4]E. Aksel and J. L. Jones, Sensors **10**(3), 1935 (2010).
[5]K. Reichmann, A. Feteira, and M. Li, Materials **8**(12), 8467–8495 (2015).
[6]Y. Zhang, X. Liu, G. Wang, Y. Li, S. Zhang, D. Wang, and H. Sun, J. Alloys Compd. **825**, 154020 (2020).
[7]A. R. Paterson, H. Nagata, X. Tan, J. E. Daniels, M. Hinterstein, R. Ranjan, P. B. Groszewicz, W. Jo, and J. L. Jones, MRS Bull. **43**(8), 600–606 (2018).
[8]P. A. Thomas, J. Kreisel, A. M. Glazer, P. Bouvier, Q. Jiang, and R. Smith, Z. Kristallogr. **220**(8), 717–725 (2005).
[9]S. Gorfman and P. A. Thomas, J. Appl. Crystallogr. **43**(6), 1409–1414 (2010).
[10]Y. Liu, R. L. Withers, J. Wang, L. Noren, A. J. Studer, and Y. Li, J. Adv. Dielectr. **02**(04), 1230012 (2012).
[11]J. Kreisel, A. M. Glazer, P. Bouvier, and G. Lucazeau, Phys. Rev. B **63**(17), 174106 (2001).
[12]D. J. Goossens, Acc. Chem. Res. **46**(11), 2597–2606 (2013).
[13]K. Riess, N. H. Khansur, A. Martin, A. Benčan, H. Uršič, and K. G. Webber, Phys. Rev. B **103**(9), 094113 (2021).
[14]G. A. Smolenskii, V. A. Isupov, A. I. Agranovskaya, and N. N. Krainik, Sov. Phys. Solid State **2**, 2982 (1960).
[15]S. B. Vakhrushev, V. A. Isupov, B. E. Kvyatkovsky, N. M. Okuneva, I. P. Pronin, G. A. Smolensky, and P. P. Syrnikov, Ferroelectrics **63**(1), 153–160 (1985).
[16]D. S. Keeble, E. R. Barney, D. A. Keen, M. G. Tucker, J. Kreisel, and P. A. Thomas, Adv. Funct. Mater. **23**(2), 185–190 (2012).
[17]T.-M. Usher, I. Levin, J. E. Daniels, and J. L. Jones, Sci. Rep. **5**, 14678 (2015).
[18]E. Aksel, J. S. Forrester, J. C. Nino, K. Page, D. P. Shoemaker, and J. L. Jones, Phys. Rev. B **87**(10), 104113 (2013).
[19]P. Thomas, S. Trujillo, M. Boudard, S. Gorfman, and J. Kreisel, Solid State Sci. **12**(3), 311 (2010).
[20]D. Schütz, M. Deluca, W. Krauss, A. Feteira, T. Jackson, and K. Reichmann, Adv. Funct. Mater. **22**(11), 2285–2294 (2012).
[21]R. Beanland and P. A. Thomas, Scr. Mater. **65**(5), 440–443 (2011).
[22]J. E. Daniels, W. Jo, and W. Donner, J. Miner., Met. Mater. Soc. 64, 1–7 (2012).
[23]J. Kreisel, P. Bouvier, B. Dkhil, P. Thomas, A. Glazer, T. Welberry, B. Chaabane, and M. Mezouar, Phys. Rev. B **68**, 014113 (2003).
[24]R. Beanland and P. A. Thomas, Phys. Rev. B **89**(17), 174102 (2014).
[25]D. K. Khatua, A. Mishra, N. Kumar, G. D. Adhikary, U. Shankar, B. Majumdar, and R. Ranjan, Acta Mater. **179**, 49–60 (2019).
[26]A. Mishra, D. K. Khatua, A. De, B. Majumdar, T. Fromling, and R. Ranjan, Acta Mater. **164**, 761–775 (2019).
[27]Y. S. Sung, J. M. Kim, J. H. Cho, T. K. Song, M. H. Kim, H. H. Chong, T. G. Park, D. Do, and S. S. Kim, Appl. Phys. Lett. **96**(2), 022901 (2010).
[28]Y. S. Sung, J. M. Kim, J. H. Cho, T. K. Song, M. H. Kim, and T. G. Park, Appl. Phys. Lett. **98**(1), 012902 (2011).
[29]F. Yang, M. Li, L. Li, P. Wu, E. Pradal-Velázquez, and D. C. Sinclair, J. Mater. Chem. A **6**(13), 5243–5254 (2018).
[30]M. Li, M. J. Pietrowski, R. A. De Souza, H. Zhang, I. M. Reaney, S. N. Cook, J. A. Kilner, and D. C. Sinclair, Nat. Mater. **13**(1), 31–35 (2014).
[31]L. Smith, T. Ibn-Mohammed, F. Yang, I. M. Reaney, D. C. Sinclair, and S. C. L. Koh, Appl. Energy **235**, 1300–1313 (2019).
[32]F. Yang, A. R. West, and D. C. Sinclair, Phys. Chem. Chem. Phys. **22**, 20941 (2020).
[33]M. Li, H. Zhang, S. N. Cook, L. Li, J. A. Kilner, I. M. Reaney, and D. C. Sinclair, Chem. Mater. **27**(2), 629–634 (2015).
[34]C. S. Lynch, Acta Mater. **44**(10), 4137–4148 (1996).
[35]W. J. Merz, Phys. Rev. **78**(1), 52–54 (1950).
[36]A. B. Kounga Njiwa, E. Aulbach, T. Granzow, and J. Rödel, Acta Mater. **55**(2), 675–680 (2007).
[37]F. H. Schader, Z. Wang, M. Hinterstein, J. E. Daniels, and K. G. Webber, Phys. Rev. B **93**(13), 134111 (2016).
[38]Y. Ehara, N. Novak, A. Ayrikyan, P. T. Geiger, and K. G. Webber, J. Appl. Phys. **120**(17), 174103 (2016).
[39]R. Garg, B. N. Rao, A. Senyshyn, P. S. R. Krishna, and R. Ranjan, Phys. Rev. B **88**, 014103 (2013).

[40]K. G. Webber, M. Vögler, N. H. Khansur, B. Kaeswurm, J. E. Daniels, and F. H. Schader, Smart Mater. Struct. **26**(6), 063001 (2017).
[41]T. Kawada, S. Watanabe, S.-I. Hashimoto, T. Sakamoto, A. Unemoto, M. Kurumatani, K. Sato, F. Iguchi, K. Yashiro, K. Amezawa, K. Terada, M. Kubo, H. Yugami, T. Hashida, and J. Mizusaki, ECS Trans. **25**(2), 467–472 (2019).
[42]K. Kwok, P. S. Jørgensen, and H. L. Frandsen, J. Am. Ceram. Soc **98**(9), 2873–2880 (2015).
[43]J. Wei, "Mechanical characterization of solid oxide fuel cells and sealants," Ph.D. thesis (RWTH Aachen University, 2017).
[44]J. Schindelin, I. Arganda-Carreras, E. Frise, V. Kaynig, M. Longair, T. Pietzsch, S. Preibisch, C. Rueden, S. Saalfeld, B. Schmid, J.-Y. Tinevez, D. J. White, V. Hartenstein, K. Eliceiri, P. Tomancak, and A. Cardona, Nat. Methods **9**, 676 (2012).
[45]F. H. Schader, E. Aulbach, K. G. Webber, and J. G. A. Rossetti, J. Appl. Phys. **113**(17), 174103 (2013).
[46]A. J. Studer, M. E. Hagen, and T. J. Noakes, Physica B **385**, 1013–1015 (2006).
[47]A. Bruker, *User's Manual* (Bruker AXS, Karlsruhe, 2014).
[48]H. D. Megaw and C. N. W. Darlington, Acta Crystallogr. Sect., A **31**(2), 161–173 (1975).
[49]I.-T. Seo, S. Steiner, and T. Frömling, J. Eur. Ceram. Soc. **37**(4), 1429–1436 (2017).
[50]R. Bhattacharyya, S. Das, and S. Omar, Acta Mater. **159**, 8–15 (2018).
[51]T. Stoto, M. Nauer, and C. Carry, J. Am. Ceram. Soc. **74**(10), 2615–2621 (1991).
[52]X. Huang, "Sintering kinetics and properties of highly pure lead zirconate titanate ceramics," Ph.D. thesis (University of Bayreuth, 2009).
[53]D. U. Seifert, L. Li, K. Y. Lee, M. J. Hoffmann, D. C. Sinclair, and M. Hinterstein, J. Eur. Ceram. Soc. **41**(2), 1221–1229 (2021).
[54]G. Arlt, D. Hennings, and G. de With, J. Appl. Phys. **58**(4), 1619 (1985).
[55]K. Riess, N. H. Khansur, A. Martin, A. Benčan, H. Uršič, and K. G. Webber, Phys. Rev. B **103**(9), 094113, (2021).
[56]J. Suchanicz and W. S. Ptak, Ferroelectr. Lett. Sect. **12**(3), 71–78 (1990).
[57]J. Suchanicz and J. Kwapulinski, Ferroelectrics **165**(1), 249–253 (1995).
[58]H. Kungl and M. J. Hoffmann, Acta Mater. **55**, 5780 (2007).
[59]K. G. Webber, E. Aulbach, T. Key, M. Marsilius, T. Granzow, and J. Rödel, Acta Mater. **57**(15), 4614–4623 (2009).
[60]E. Aksel, J. S. Forrester, B. Kowalski, J. L. Jones, and P. A. Thomas, Appl. Phys. Lett. **99**(22), 222901 (2011).
[61]E. Aksel, J. S. Forrester, B. Kowalski, M. Deluca, D. Damjanovic, and J. L. Jones, Phys. Rev. B **85**(2), 024121 (2012).
[62]M. J. Hoffmann, M. Hammer, A. Endriss, and D. C. Lupascu, Acta Mater. **49**, 1301 (2001).
[63]G. Picht, N. H. Khansur, K. G. Webber, H. Kungl, M. J. Hoffmann, and M. Hinterstein, J. Appl. Phys. **128**(21), 214105 (2020).
[64]A. Glazer, Acta Crystallogr., Sect. B: Struct. Sci. **28**(11), 3384–3392 (1972).
[65]J. Frantti, S. Ivanov, S. Eriksson, H. Rundlöf, V. Lantto, J. Lappalainen, and M. Kakihana, Phys. Rev. B **66**(6), 064108 (2002).
[66]G. Jones and P. Thomas, Acta Crystallogr., Sect. B: Struct. Sci. **58**(2), 168–178 (2002).
[67]S. Kong, N. Kumar, S. Checchia, C. Cazorla, and J. Daniels, Adv. Funct. Mater. **29**(27), 1900344 (2019).
[68]G. Jones and P. Thomas, Acta Crystallogr., Sect. B: Struct. Sci. **56**(3), 426–430 (2000).
[69]G. C. Kostogloudis and C. Ftikos, Solid State Ionics **126**(1–2), 143–151 (1999).
[70]J.-J. Zhou, J.-F. Li, and X.-W. Zhang, J. Eur. Ceram. Soc. **32**(2), 267–270 (2012).
[71]F. Chen, Y.-H. Li, G.-Y. Gao, F.-Z. Yao, K. Wang, J.-F. Li, X.-L. Li, X.-Y. Gao, and W. Wu, J. Am. Ceram. Soc. **98** (4), 1372—1376 (2015).
[72]T. Leist, T. Granzow, W. Jo, and J. Rödel, J. Appl. Phys. **108**(1), 014103 (2010).
[73]T. Leist, K. G. Webber, W. Jo, E. Aulbach, J. Rödel, A. D. Prewitt, J. L. Jones, J. Schmidlin, and C. R. Hubbard, Acta Mater. **58**(18), 5962–5971 (2010).
[74]G. Wang, A. Goetzee-Barral, Z. Lu, D. S. Keeble, and D. A. Hall, J. Eur. Ceram. Soc. **41**(6), 3832–3837 (2021).
[75]X. Shi, N. Kumar, and M. Hoffman, J. Mater. Chem. C **6**(45), 12224–12233 (2018).
[76]Z. Zhao, X. Liang, T. Zhang, K. Hu, S. Li, and Y. Zhang, J. Eur. Ceram. Soc. **40**(3), 712–719 (2020).
[77]M. Kuhn, S. Hashimoto, K. Sato, K. Yashiro, and J. Mizusaki, Solid State Ionics **241**, 12–16 (2013).
[78]B. Kaeswurm, F. H. Schader, and K. G. Webber, Ceram. Int. **44**(2), 2358–2363 (2018).
[79]S. Zhang, F. Li, N. P. Sherlock, J. Luo, H. Jae Lee, R. Xia, R. J. Meyer, W. Hackenberger, and T. R. Shrout, J. Cryst. Growth **318**(1), 846–850 (2011).
[80]A. Martin, K. Kakimoto, K. Hatano, Y. Doshida, and K. G. Webber, J. Appl. Phys. **122**(20), 204102 (2017).
[81]A. Pramanick, D. Damjanovic, J. E. Daniels, J. C. Nino, and J. L. Jones, J. Am. Ceram. Soc. **94**, 293 (2011).
[82]V. S. Postnikov, V. S. Pavlov, and S. K. Turkov, J. Phys. Chem. Solids **31**(8), 1785–1791 (1970).
[83]M. I. Morozov, M.-A. Einarsrud, J. R. Tolchard, P. T. Geiger, K. G. Webber, D. Damjanovic, and T. Grande, J. Appl. Phys. **118**(16), 164104 (2015).
[84]Y.-K. Choi, T. Hoshina, H. Takeda, T. Teranishi, and T. Tsurumi, Appl. Phys. Lett. **97**(21), 212907 (2010).
[85]L.-X. He, C.-E. Li, Z.-Y. Wang, H.-X. Yan, and W. Liu, Phys. Status Solidi A **179**(1), 275–283 (2000).
[86]Z. Zhang, J. Koppensteiner, W. Schranz, D. Prabhakaran, and M. A. Carpenter, J. Phys.: Condens. Matter **23**(14), 145401 (2011).
[87]W. Liang, D. Xiao, W. Wu, X. Li, Y. Sun, and J. Zhu, Curr. Appl. Phys. **11**(3, Suppl.), S138–S142 (2011).
[88]D. Shihua, S. Tianxiu, Y. Xiaojing, and L. Guanghua, Ferroelectrics **402**(1), 55–59 (2010).